Retention of Iodide and Chloride by Formation of a Green Rust Solid Solution GR-$Cl_{1-x}I_x$: A Multiscale Approach

Tim Platte,* Nicolas Finck, Stefan Mangold, Robert Polly, and Horst Geckeis

ABSTRACT: The uptake of iodide and chloride during the synthesis of green rust (GR), the Fe endmember of the layered double hydroxide (LDH) group, was investigated. GR compounds were prepared by aerial oxidation of $Fe(OH)_2$ in suspension, considering various I/Cl ratios at constant ionic strength. Only GR compounds formed in all experiments, and the associated I/Cl ratio increased with that of the starting suspension. No preferential uptake of any halide could be detected, and all compounds had comparable morphology. Furthermore, the height of the interlayer gallery increased with the I/Cl ratio from ~7.7 Å for the chloride endmember to ~8.3 Å for the iodide endmember, and the observed linear increase was attributed to increasing interlayer iodide content. In all compounds, Fe K edge X ray absorption spectroscopy evidenced the presence of sixfold coordinated iron with a Fe^{2+}/Fe^{3+} ratio of 3, homogeneously distributed within flattened octahedral sites, with six Fe as next nearest neighbors. The Fe short range environment was not affected by the interlayer composition, and no halide from the interlayer could be detected. Furthermore, iodide and chloride anions are located in a water like environment, being loosely bound by weak electrostatic interactions to the octahedral sheet likely above ferric iron. Results consistently hint at the formation of a solid solution between chloride and iodide GR endmembers, certainly facilitated by the crystallization of both compounds in the same space group. This study provides further insights into the ability of LDH to simultaneously accommodate several anionic species of various sizes. The formation of such LDH compounds in a deep geological repository for nuclear waste thus represents a possible retention barrier to the migration to the far field of anionic species like $^{36}Cl^-$ and $^{129}I^-$ mobilized from the waste matrix. The extent of retention in disposal sites will depend, among others, on the availability of GR and on the concentration of competing anions.

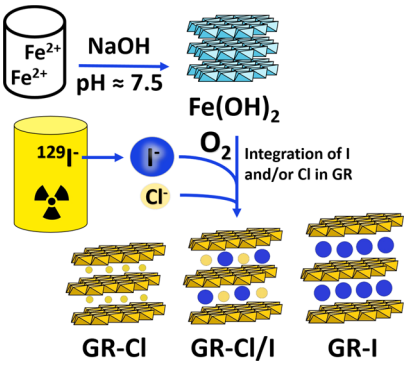

1. INTRODUCTION

Iodine occurs in nature and is an essential trace element for living organisms. Besides very minor generation by cosmic radiation, radioactive iodine has anthropogenic sources such as atmospheric testing of nuclear weapons, reprocessing of spent nuclear fuel, and nuclear accidents (Chernobyl, Fukushima Daiichi).[1] Release of radioisotopes of iodine [^{131}I ($t_{1/2} \approx 8$ d) and ^{129}I ($t_{1/2} \approx 15.7$ Ma)] can have negative health effects on humans because of radiological hazards when taken up by the thyroid at relevant levels. Iodine is also present in high level nuclear waste that is foreseen to be encapsulated in steel canisters and disposed of in deep geological repositories (DGRs).[2] Upon release from the nuclear waste matrix in case of canister failure, iodine is expected to prevail as iodide (I^-) because of the reducing conditions expected to develop in a DGR and may therefore be only poorly retained in the repository near field by the geotechnical barrier (e.g., bentonite).[3−7]

Under repository relevant conditions, steel corrosion will result in the formation of Fe(II) bearing phases such as green rust (GR) compounds.[8−10] GR is the Fe endmember of the layered double hydroxide (LDH) group and bears a permanent positive charge that is balanced by hydrated interlayer anions. The general structural formula of GR can be written as $[Fe(II)_{1-x}Fe(III)_x(OH)_2]^{x+}$ $[(x/n)A^{n-}, mH_2O]^{x-}$, where A denotes the intercalated anions and x represents the fraction of ferric iron. The structure and composition of GR depend on the nature of intercalated anions.[11−14] Spherical or planar anions such as Cl^- or CO_3^{2-} lead to GR type 1 having a rhombohedral unit cell consisting of three repeat units with hydroxide sheets separated by interlayers composed of one plane of anions and water molecules. Three dimensional anions such as SO_4^{2-} lead to GR type 2 having a hexagonal unit cell consisting of two repeat units, and the interlayer is composed of two adjacent planes of anions and water molecules. LDH and thus GR compounds are also known as anionic clays, meaning that the intercalated anionic species can be exchanged for negatively charged species present in the

contacting solution. GR may therefore have the capability to bind dissolved anionic species such as iodide, which may be mobilized upon waste matrix alteration[15−18] in a DGR or present in the environment.[19,20]

Owing to the ubiquitous presence of chloride ions in the environment and to its well known reactivity, the chloride containing GR (GR Cl) should be considered as a phase commonly occurring upon iron corrosion in various suboxic and anoxic environments.[21] Indeed, the formation of GR Cl as a steel corrosion product under anoxic, high saline, and elevated temperature conditions in the laboratory has been observed,[22,23] and thus, this phase is to be expected in scenarios assuming corroding metallic containers in a DGR in rock salt formations. Depending on the availability of other anions (e.g., carbonate), GR CO_3 can also be encountered frequently.[14,24]

GR compounds can be formed via different biotic and abiotic pathways.[25] In the laboratory, the simplest way to synthesize GR is by direct precipitation from ferric and ferrous salts under anoxic conditions. Alternatively, the partial oxidation of ferrous hydroxide in suspension, the interaction of aqueous Fe(II) with ferric (oxyhydr)oxides, or the electrochemical oxidation of zerovalent iron can also result in the formation of GR. GR chloride can also form under conditions more representative of nuclear waste disposal, such as upon interaction between Fe^{2+} formed by steel corrosion and smectite present in bentonite,[26,27] the oxidation of $Fe(OH)_2$ forming upon steel corrosion by reaction with water hydrolysis species (e.g., O_2 and H_2O_2), or by the establishment of appropriate oxidation−reduction potentials.

The synthesis in the laboratory of LDH, such as AFm phases (hydrated calcium aluminates) and GR compounds, containing halides is well established.[28−30] In all studies, the basal spacing increases with the size of the intercalated hydrated anion without significantly affecting the octahedral sheet. AFm phases occur mainly in hydrated cement paste and are composed of hydroxide layers made of edge sharing Ca^{2+} and Al^{3+}/Fe^{3+} octahedra.[31] When synthesized in the simultaneous presence of I^- and SO_4^{2-}, a solid solution forms between AFm I_2 and AFm SO_4 endmembers.[29] More recently, Nedyalkova et al. (2020) reported the formation of extensive solid solutions between the monoiodide and hydroxy AFm and between the monoiodide and hemi carbonate AFm endmembers, respectively.[32] In both studies, the respective endmembers of the investigated solid solutions have a similar crystal symmetry, which favors the formation of solid solutions that was evidenced by a gradual change in basal reflection from one endmember to the other. Uptake studies of anionic species by preformed LDH compounds have also been reported. For example, iodide can be taken up by GR Cl or by ZnAl LDH via an ion exchange mechanism, despite the difference in ionic radii.[33,34] In the study with GR Cl, it was further suggested that iodide containing GR (GR I) would form, but the formation of such a compound or of a GR compound containing both halides was not demonstrated. In contrast, in the study with ZnAl LDH, the presence of both halides was demonstrated by fits to the X ray powder diffractogram. More recently, Agnel et al. (2020) showed that chloride can be replaced by sulfate within GR interlayers, resulting in the formation of separate chloride and sulfate containing GR, without solid solution formation.[35] All these studies suggest that the formation of a solid solution is favored only when endmembers crystallize in the same space group. Finally, GR compounds containing either bromide or iodide in the interlayer have been prepared in the laboratory,[28] and these compounds are isostructural with the chloride containing GR endmember. Results showed a progressive increase in basal spacing with the size of intercalated halide without affecting the brucitic sheet. The simultaneous intercalation of halides of various sizes within the interlayer of GR may thus be possible, and a solid solution may form, but this still needs to be demonstrated.

The goal of this study was to investigate the uptake mechanism of chloride and iodide during the formation of GR compounds in the presence of both anions. A series of GR compounds was prepared, the uptake was quantified and the nature of the formed solid phases was characterized at various scales to determine whether GR containing simultaneously both halogen form or if separate chloride and iodide containing GR form. To this end, GR compounds have been synthesized at constant ionic strength of halides and for varying chloride to iodide ratios. The amounts of chloride and iodide taken up were determined by quantification of the supernatants, and the nature and composition of the synthesized compounds were characterized by X ray diffraction (XRD) and by scanning electron microscopy (SEM)−energy dispersive X ray spectroscopy (EDX). In addition, short range information on the organization of the octahedral sheet and of the interlayer was provided by X ray absorption spectroscopy (XAS) at the Fe K edge, I L_3 edge, and Cl K edge. Specifically, extended X ray absorption fine structure (EXAFS) spectros copy at the Fe K edge was used to verify if the presence of a heavy backscattering atom like iodine in the interlayer would be detectable in the EXAFS spectra and so inform on the strength of the interaction between intercalated anions and the octahedral sheet. The present work aims at developing a comprehensive understanding of the iodide uptake mechanism by GR compounds by combining long range (i.e., XRD) and short range (i.e., XAS) scale information.

2. MATERIALS AND METHODS

2.1. Sample Preparation. All samples were prepared with ultrapure water (UPW, 18.2 MΩ cm, Milli Q system, Millipore) and reagents of ACS grade or higher. The sources of Fe(II), Cl(I), and I(I) were $FeCl_2{\cdot}4H_2O$, NaCl, and NaI, respectively. Unless otherwise indicated, all steps from sample preparation to analysis were performed under anoxic conditions (e.g., Ar filled glovebox, <1 ppmv O_2). pH values were measured with a combined pH electrode that was calibrated before every use (pH buffers 4, 7, 10). E_h values were recorded using a Pt Ag/AgCl electrode and corrected versus SHE. The suspensions were stirred during E_h and pH measurements.

All GR samples have been prepared using $Fe(OH)_2$ as the precursor phase.[36] $Fe(OH)_2$ was prepared by titrating a stirred 0.14 M $FeCl_2{\cdot}4H_2O$ solution with a 1 M NaOH solution until pH 7.5. Chloride anions were removed by centrifuging the suspension for 10 min at 3500 rpm (2000*g*) and replacing the supernatant by UPW. After the second centrifugation step, the supernatant was replaced by a solution containing a mixture of chloride and iodide ions, keeping the ionic strength constant at 0.275 mol/L (Table 1). Samples were transferred to an Ar filled glovebox, and the conversion to GR was initiated by pumping air into the containers for 4−5 s (∼10 L/min). The air was first purged of CO_2 by bubbling through 1 M NaOH, and then, the air was cleaned of NaOH and humidified by bubbling through UPW. These conditions of air flow deviate from that applied by, for example, Christiansen et al. (2009) but were successful in preparing GR without any other admixed phase, and pH and E_h values in suspension were comparable to that reported for GR Cl prepared by direct precipitation.[6] GR samples were subsequently transferred

Table 1. Chemical Conditions Used to Prepare the Samples and Relative Halogen Content in GR Compounds as Determined by SEM−EDX[a]

sample	Cl_i/I_i in solution [mol/mol]	Cl_f/I_f in GR [mol/mol]	distribution coefficient K_{SW}	R_d [L/g]
GR-Cl	100:0	100:0		0.005(2)
GR-$Cl_{0.9}I_{0.1}$	90:10	88:12(3)	0.109(5)	
GR-$Cl_{0.7}I_{0.3}$	70:30	76:24(3)	0.067(3)	
GR-$Cl_{0.5}I_{0.5}$	50:50	58:42(3)	0.071(4)	
GR-$Cl_{0.3}I_{0.7}$	30:70	38:62(3)	0.076(4)	
GR-$Cl_{0.1}I_{0.9}$	10:90	9:91(3)	0.088(4)	
GR-I	0:100	4:96(3)[b]	0.083(4)	

[a]Subscripts i and f denote initial and final Cl^- and I^- concentrations in solution at equilibrium, respectively. The total initial halide concentration was 0.275 ± 0.02 mol/L. pH_f = 7.3, E_{hf} = −310 ± 40 mV, and c(GR) = 22 ± 5 mmol/L. Uncertainties are indicated in parentheses. [b]GR I contains low levels of chloride left because chloride could not be removed quantitatively by washing the $Fe(OH)_2$ suspension.

back to the glovebox before further analysis. Finally, the iodine uptake was quantified by calculating R_d and distribution coefficient K_{sw} as

$$R_d = R_d[\mathrm{L/g}] = \left(\frac{c_0 - c_L}{c_L}\right) * \frac{V[\mathrm{L}]}{m[\mathrm{g}]} \quad (1)$$

where c_0 is the initial concentration of the sorbing substance, c_L is the concentration of the sorbing substance at equilibrium, V is the volume of the system, and m is the mass of the solid phase. The distribution coefficient K_{sw} was calculated as

$$K_{SW} = \frac{c_1}{c_2} \quad (2)$$

where c_1 is the final concentration of I^- in GR and c_2 is the final concentration of I^- remaining in the supernatant at equilibrium.

2.2. Solid Phase Characterization. For the analysis of GR compounds (XRD, SEM−EDX, and XAS), a small amount of the sample slurry was centrifuged in the glovebox at 13,000 rpm for 15 min. The supernatant was removed and replaced by UPW twice. This procedure of sample preparation was applied before each analysis, and only freshly prepared samples were used in all analyses. Consequently, if the presence of salt crystallizing upon slurry drying is suggested by, for example, XRD analysis, it does not necessarily imply that this salt is present in the sample used, for example, for XAS analysis (and vice versa).

Samples for XRD analysis were oriented mounts prepared by drying sample slurry on a low background and airtight sample holder. X ray powder diffractograms were recorded using a D8 ADVANCE (Bruker) diffractometer equipped with a Cu Kα source and a LynxEye XE T detector. Crystalline phases were identified by comparison with the PDF 2 database using the DIFFRAC.EVA v5.0 software (Bruker), and fits to the experimental powder patterns were obtained using the DIFFRAC.TOPAS v6.0 software (Bruker). Samples for SEM−EDX analysis were prepared by drying a small amount of slurry on a holder, which was transported to the microscope under anoxic conditions and then quickly positioned in the microscope to minimize the exposure time to air. Information on size and morphology of particles was provided by scanning electron microscopy [Quanta 650 FEG (FEI)], and information on chemical composition was provided by EDX.

2.3. X-ray Absorption Spectroscopy. Fe K edge, I L_3 edge, and Cl K edge X ray absorption spectra were recorded at room temperature at the XAS beamline at the KIT synchrotron light source (Karlsruhe Institute of Technology, Germany) with a storage ring energy of 2.5 GeV. The energy of the incident X ray beam was monochromatized using a Si(111) double crystal monochromator. At the Fe K edge, the energy was calibrated by assigning the first inflection of the Fe K edge XANES recorded on an Fe foil measured in parallel with all samples to 7112.0 eV. At the I L_3 edge and at the Cl K edge, the energy was calibrated by assigning the first inflection point of the Sn L_1 edge recorded on a Sn foil to 4465 eV. Data were recorded either in transmission mode using ionization chambers filled with appropriate mixtures of He, N_2, and Ar gases or in fluorescence yield mode using a silicon drift detector (Vortex, SII Nano Technology). Adequate counting statistics was achieved by recording 3 to 11 scans per edge and per sample.

Samples were prepared in the Ar filled glovebox by sealing dry powder between two layers of Kapton tape (70 μm thickness) and mounted on a holder located in an airtight transport box. At the beamline, the transport box was connected to the measuring chamber, the chamber was purged several times with N_2 before the port between the chamber and box was opened, and the holder was introduced inside the chamber. Spectra were recorded considering an angle of ∼35° between the electric field of the X ray beam and the sample plane to avoid texture effects.[37,38] Magnetite, $FeCl_2{\cdot}4H_2O$, $FeCl_3$, aqueous NaI solution ($NaI_{(aq)}$), and NaCl (crystalline $NaCl_{(cr)}$ and aqueous $NaCl_{(aq)}$) were used as reference compounds, and Fe K edge data of magnetite were recorded at the INE beamline.[39]

XAS data were analyzed following standard procedures by using the Athena and Artemis interfaces in the Ifeffit software.[40] Fe K edge and

Table 2. Quantitative EXAFS Analysis of Samples and Reference Compounds at the Fe K Edge

sample	FT range[a] [Å^{-1}]	fit range[b] [Å]	shell	N	d [Å]	σ^2 [Å^2]	ΔE_0 [eV]	R_f
GR-Cl	4.0 14.0	1.2 3.25	O_1	6	2.11(2)	0.012(2)	3.6	0.007
			Fe_1	6	3.20(2)	0.009(2)		
GR-$Cl_{0.9}I_{0.1}$	4.0 14.0	1.2 3.25	O_1	6	2.09(2)	0.011(2)	3.0	0.015
			Fe_1	6	3.20(2)	0.008(2)		
GR-$Cl_{0.7}I_{0.3}$	4.0 14.0	1.2 3.25	O_1	6	2.09(2)	0.011(2)	2.8	0.016
			Fe_1	6	3.20(2)	0.007(2)		
GR-$Cl_{0.5}I_{0.5}$	4.0 14.0	1.2 3.25	O_1	6	2.09(2)	0.012(2)	2.8	0.014
			Fe_1	6	3.20(2)	0.008(2)		
GR-$Cl_{0.3}I_{0.7}$	4.0 14.0	1.2 3.25	O_1	6	2.09(2)	0.012(2)	2.3	0.016
			Fe_1	6	3.20(2)	0.009(2)		
GR-$Cl_{0.1}I_{0.9}$	4.0 14.0	1.2 3.25	O_1	6	2.09(2)	0.012(2)	3.0	0.015
			Fe_1	6	3.20(2)	0.008(2)		
GR-I	4.0 14.0	1.2 3.25	O_1	6	2.10(2)	0.012(2)	2.8	0.012
			Fe_1	6	3.21(2)	0.008(2)		

[a]Fourier transformed range. [b]$R + \Delta R$ interval for the fit. N is the coordination number (fixed), d is the interatomic distance, σ^2 is the mean squared displacement (Debye−Waller term), ΔE_0 is the shift in ionization energy with E_0 threshold energy taken as maximum of the first derivative, and R_f is the figure of merit of the fit as reported in Finck et al. (2015). Uncertainties are indicated in parentheses.

I L_3 edge EXAFS spectra ($\chi(k)$) were extracted from raw data, and Fourier transforms (FTs) were obtained from the $k^3 \times \chi(k)$ functions. Data were fit in R space using phase and amplitude functions calculated with feff6.0.[41] Fe K edge EXAFS data were modeled using theoretical paths generated using the published structure of GR,[42] with the amplitude reduction factor (S_0^2) fixed at 0.86.[26] Iodine L_3 edge EXAFS spectra were modeled using single scattering paths, with S_0^2 set to 1.0.[43] Uncertainties on bond distances and coordination numbers are indicated in parentheses in Table 2. The quality of the fit was quantified by the R_f factor, which represents the absolute misfit between theory and data.

3. RESULTS AND DISCUSSION

3.1. GR Morphology and Iodine Uptake. All synthesized compounds have a comparable morphology. They have a layered structure and are made of thin hexagonal platelets, which is typical of GR compounds (Figure 1). Platelets have

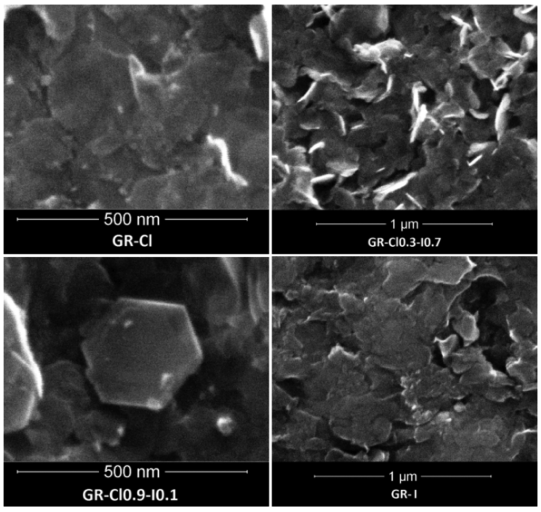

Figure 1. Scanning electron micrographs of GR Cl (top left), GR $Cl_{0.3}I_{0.7}$ (top right), GR $Cl_{0.9}I_{0.1}$ (bottom left), and GR I (bottom right).

sizes up to several hundreds of nanometers in width and several tens of nanometers in thickness. These results compare well with GR Cl prepared by direct precipitation from Fe salts.[6] No particle of other morphology could be detected on the micrographs, ruling out the presence of, for example, magnetite in substantial amounts.

Information on elemental composition was provided by EDX analysis (Table 1). In all samples, the Cl/I molar ratio associated with GR platelets was close to the value of the suspension, from which they were prepared. This result suggests that under the given experimental conditions (similar pH and E_h values, same starting total halide concentration and GR content), there is no significant preferential uptake of any specific halide and thus that the composition of the interlayer directly depends on the atomic ratio in solution. The atomic ratio in GR I slightly deviates from that of the set ionic strength during synthesis and can be attributed to non quantitative removal of chloride during washing of the precursor phase. For all samples, R_d values are rather low and comparable (Table 1). Interestingly, R_d determined in this study (R_d = 0.005 L/g) is somewhat lower but comparable to reported values for iodide retained by AFm phases (0.026 ± 0.003 L/g, ionic strength significantly lower).[29] This finding may suggest that the uptake of iodide by LDH phases is not significantly affected by the composition of the octahedral sheet.

3.2. XRD Analysis. The X ray diffractograms of all synthesized GR compounds are consistent with the presence of GR only, and no other crystalline Fe phase could be detected (Figure 2). This implies a quantitative conversion of the $Fe(OH)_2$ precursor phase and the absence of admixed oxidation products such as magnetite. All diffractograms exhibit only two reflections related to the (003) (d_{003}, 1/3c) and (006) (d_{006}, 1/6c) basal spacings (the full diffractogram of all samples can be found in Supporting Information). d_{003} is the basal repeat distance and equals the thickness of the brucitic like layer plus interlayer. d_{006} equals half of d_{003}; thus, it represents the distance until the center of interlayer gallery. Because GR compounds have a layered structure, the protocol used to prepare samples provides a high degree of particle orientation parallel to the surface of the holder (i.e., texture), and thus, patterns display only basal reflections (d_{003} and d_{006}). The position of both basal spacings continuously shifts to lower angles from GR Cl to GR I (i.e., with the increasing iodide/chloride ratio in the starting suspension, Table 1), which indicates an increase in both d_{003} and d_{006}. The observed increase in basal spacings can be attributed to an increase of the interlayer thickness that can best be explained by the presence of both iodide and chloride within the interlayer. Phase segregation, that is, the formation of separate GR Cl and GR I phases, and interstratification, that is, regular stacking of interlayers alternatively filled with Cl^- and I^-, can both be dismissed, as these would have been evidenced by the presence of different sets of d_{003} and d_{006} and additional reflections. In contrast, data rather suggest the formation of a solid solution between the chloride and iodide endmembers, facilitated by the crystallization of both endmembers in the same space group ($R3m$).

Modeling of experimental diffractograms reveals a gradual increase from d_{003} = 7.72 Å and d_{006} = 3.88 Å in GR Cl to d_{003} = 8.29 Å and d_{006} = 4.16 Å in GR I (Figure 2). The presence of both separate GR Cl and GR I in GR Cl_xI_{1-x} samples was tested by modeling experimental diffractograms using reflections located at positions corresponding to that of the endmembers. This hypothesis was ruled out based on the significant misfit between experimental and modeled data (Supporting Information). Consequently, GR samples prepared in the presence of both anions are not mechanical mixtures of separate GR Cl and GR I compounds, but results strongly point at the formation of GR compounds containing both halides within the interlayer. This behavior is comparable to that reported for ZnAl LDH: d_{003} increased from 7.74 Å for the chloride containing compound to 8.10 Å for the compound obtained after exchanging ~60% of Cl^- for I^-, resulting in a random distribution of both anions within the interlayer without forming a separate phase.[34] The presence of both halides in the GR interlayers is further supported, considering reported data for AFm phases.[32] Despite the significant difference in the ionic radius[44] between iodide (2.20 Å) and hydroxyl anions (1.37 Å), the formation of an extensive solid solution was observed between the monoiodide and hydroxy AFm endmembers. Because the size mismatch between I^- and Cl^- is much smaller than that between I^- and OH^-, it is reasonable to assume the formation of a solid solution between GR Cl and GR I endmembers. The presence of minute amounts of admixed separate GR Cl and/or GR I up to the detection limit cannot be ruled out.

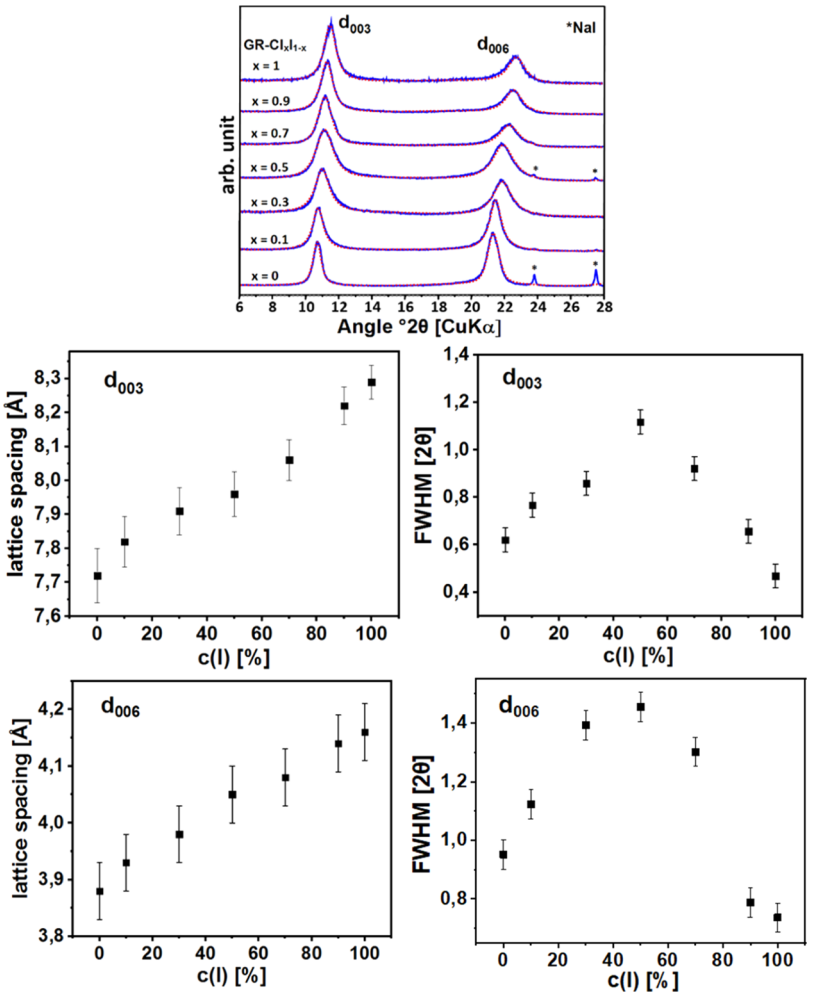

Figure 2. Top: experimental (blue line) and modeled (red line) X ray diffractogram of GR Cl_xI_{1-x} ($0 \leq x \leq 1$) samples. Middle: d_{003} basal spacing (left) and full width at half maximum (fwhm) (right) as a function of the amount of I^- in solution. Bottom: d_{006} basal spacing (left) and fwhm (right) as a function of the amount of I^- in solution.

For the endmembers, values of basal spacings obtained from fits to experimental data agree within uncertainties with reported data.[21,28] Assuming a thickness of the octahedral sheet of ~2 Å, these values indicate an increase in height of the interlayer gallery from ~5.7 to ~6.3 Å, which parallels the increase in ionic diameter from 3.62 Å (Cl^-) to 4.40 Å (I^-).[44] To achieve incorporation of both chloride and iodide within the interlayer without forming a separate phase, results may suggest a structural arrangement of water molecules around iodide, possibly differing from that around chloride or a possibly slightly different location of both halides within the interlayer. The crystal structure of GR Cl can be considered analogous to that of iowaite, which consists of positively charged $[Mg^{II}_3Fe^{III}(OH)_8]^+$ hydroxide sheets alternating with $[Cl{\cdot}2H_2O]^-$ in the interlayer.[45] In this compound, Cl^- and water molecules are extensively disordered and located at about 0.40 Å off the threefold axis connecting two OH^- of adjacent hydroxide layers. Assuming the presence of 1.5−2 water molecules per chloride ion in the interlayer of GR Cl, Refait et al. reported a location of H_2O slightly closer to the OH−OH threefold axis than Cl^-, consistent with the smaller radius of OH^- compared to Cl^- and with experimental OH−Cl interatomic distances.[21] Because of the larger size of iodide compared to chloride, it may be assumed that I^- in GR I is located further away from the threefold axis than Cl^- in GR Cl.

On the diffractograms, the relative intensity of basal reflections (Figure 2) is also affected by the iodine content. Compared to the intensity of d_{003}, the intensity of d_{006} increases from GR Cl to GR I, that is, with the iodide content in the sample. Iodine ($Z = 53$) is significantly heavier than chlorine ($Z = 17$) and thus scatters X rays more efficiently than the lighter halide. The observed increase in relative intensity of d_{006} from GR Cl to GR I further hints at the presence of increasing iodide content within the interlayer with the increasing I/Cl ratio in the starting solution. The observed increase in relative intensity of d_{006} with the iodide content in the interlayer agrees with earlier findings on ZnAl LDH.[34]

A careful inspection of X ray diffractograms further reveals that the fwhm of d_{003} is affected by the composition of the interlayer. Fit results show a slight increase in fwhm from GR Cl to GR $Cl_{0.5}I_{0.5}$ and then a decrease from GR $Cl_{0.5}I_{0.5}$ to GR I. The fwhm of d_{006} follows the same trend, with very comparable values. There may be two possible explanations for this finding. First, the fwhm is inversely proportional to the mean size of crystallites in the direction perpendicular to the lattice planes (Scherrer equation).[46,47] Therefore, experimental data may indicate that the size of particles, more precisely the coherent scattering domain size, first decreases from GR Cl to GR $Cl_{0.5}I_{0.5}$ and then increases from GR $Cl_{0.5}I_{0.5}$ up to GR I (Figure 2). Second, the observed variations in fwhm may

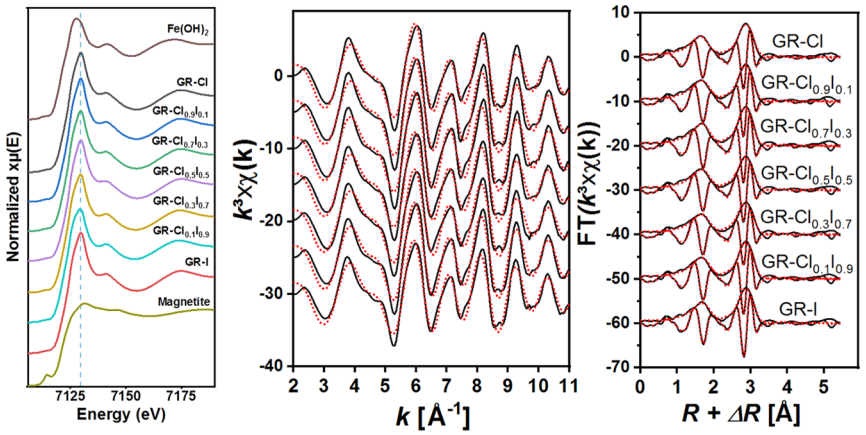

Figure 3. Fe K edge XANES (left) of the GR samples and of the magnetite and $Fe(OH)_2$ reference compounds. Experimental (solid black line) and modeled (dashed red line) EXAFS spectra (middle) with the corresponding FTs (right) of all GR samples. Fit results are present in Table 2.

originate from disorder in crystal stacks, certainly resulting from non homogeneous interlayer filling due to the simultaneous presence of anions of different sizes. In turn, this may result in a distribution of slightly different basal spacings around a mean value, and because XRD averages over the whole sample, recorded diffractograms provide information on the average basal spacing. We consider the latter explanation more plausible and do not have a rational support for a tentative crystallite size dependency of GR species on the Cl^-/I^- ratio. Results may thus suggest the formation of GR with the simultaneous presence of both halides in the interlayer, with a likely more ordered organization of interlayers close to endmembers and a more disordered one toward mixed filling (i.e., GR $Cl_{0.5}I_{0.5}$). This hypothesis would be supported by the slightly larger fwhm of d_{006} representing the distance from the octahedral Fe plane to the interlayer halide plane. Indeed, the aerial oxidation of $Fe(OH)_2$ results first in the formation of positively charged hydroxide layers containing Fe^{3+} cations, which subsequently adsorb anions and water molecules.[21] These precursors then merge alternatively during the growth of the GR microcrystals. It is very likely that the presence of either only chloride or only iodide anions favors the formation of thicker stacks of hydroxide platelets compared to the presence of both anions adsorbed at the surface of hydroxide layers.

3.3. X-ray Absorption Spectroscopy. Vibrational spectroscopic techniques (e.g., infrared spectroscopy) can be applied for the structural analysis of LDH.[25,48] An interesting alternative is the application of XAS to probe the local chemical environment of selected elements in terms of type and number of neighboring atoms, interatomic distances, and often site symmetry. In the present study, structural information at the short range scale on the octahedral sheet and on the interlayer organization was obtained by probing the Fe K edge, I L_3 edge, and Cl K edge by XAS.

3.3.1. Fe K-Edge XAS. The Fe K edge EXAFS spectrum and the corresponding FT of all samples are similar up to $R + \Delta R$ ~5.5 Å (Figure 3). Data fitting provided comparable results (Table 2), suggesting that the structure of the octahedral sheet is not affected by the composition of the interlayer. In all samples, Fe is bound to 6 O atoms at $d(Fe-O) = 2.10(2)$ Å and six next nearest Fe atoms were detected at $d(Fe-Fe) \sim 3.20(1)$ Å. Fit results agree with the reported crystallographic data of GR, confirming that Fe octahedra share edges.[21,26,49] For GR Cl and GR I, experimental bond distances further agree with recent results from theoretical calculations at the density functional theory (DFT) level.[50,51] Interestingly, the Fe K edge spectrum of GR I does not significantly differ from the spectrum of GR Cl (Cl is a light backscatterer, not detectable at large distances), which is a clear indication that there is no preferential coordination between Fe and I polyhedra. Interlayer anions are also far from Fe atoms, being screened by OH^- of the octahedral sheet.[52]

In GR compounds, $d(Fe-O)$ and $d(Fe-Fe)$ are shorter than in $Fe(OH)_2$ ($d(Fe-O) = 2.14$ Å; $d(Fe-Fe) = 3.26$ Å),[49] from which they formed. This is attributed to the presence of octahedral ferric iron in GR, which is smaller than ferrous iron. The EXAFS derived Fe−O bond distance equals 2.10 Å (Table 2), and this can be used to estimate the Fe^{2+}/Fe^{3+} ratio in the samples. For Fe^{3+} sixfold coordinated by hydroxyl, a mean bond distance of $d(Fe^{3+}-O) = 0.65 + 1.35 = 2.00$ Å would be expected,[44] which agrees with values reported for octahedral ferric iron in clay minerals.[37,38] For sixfold coordinated Fe^{2+}, the calculated bond distance equals 0.78 + 1.35 = 2.13 Å. Using these values, the experimental $d(Fe-O) =$ 2.10 Å suggests that the octahedral sheet of GR compounds is filled with about 25% of Fe^{3+} and 75% of Fe^{2+} ions (i.e., $0.25 \times 2.00 + 0.75 \times 2.13 = 2.10$ Å). The resulting Fe^{2+}/Fe^{3+} ratio of 3 agrees with reported data of freshly prepared GR Cl by aerial oxidation of $Fe(OH)_2$.[21] Furthermore, in the crystal structure of GR Cl, a and b unit cell parameters are equal and correspond to the Fe−Fe distance. Modeling of EXAFS data yielded $d(Fe-Fe) = 3.20(2)$ Å in all compounds, in agreement with reported a unit cell parameters for GR Cl and GR I.[28] In the octahedral sheet of GR compounds, next nearest cationic shells are located at $a\sqrt{3}$, $2a$, $a\sqrt{7}$, ...,[52] but no attempt was made to model Fe contributions at such large distances.

Assuming in first approximation a behavior of Cl^- in GR Cl comparable to that of Cl^- in MgAl LDH, the chloride ions and water molecules are homogeneously distributed in the center of the interlayer, the halide being stabilized by electrostatic interactions above the trivalent octahedral cation.[53] In this configuration and based on XRD results, the distance from Cl^- to Fe^{3+} would be ~3.9 Å (Table 2). Furthermore, if Cl^- anions are only loosely bound close to one quarter of octahedral sites (i.e., Fe^{3+} ions), the contribution of backscattering from the halide to the EXAFS spectrum of GR Cl is expected to be very low because the recorded spectrum corresponds to the average of all probed octahedral atoms. Yet, from GR Cl to GR I the interlayer anion becomes larger and heavier, while the distance

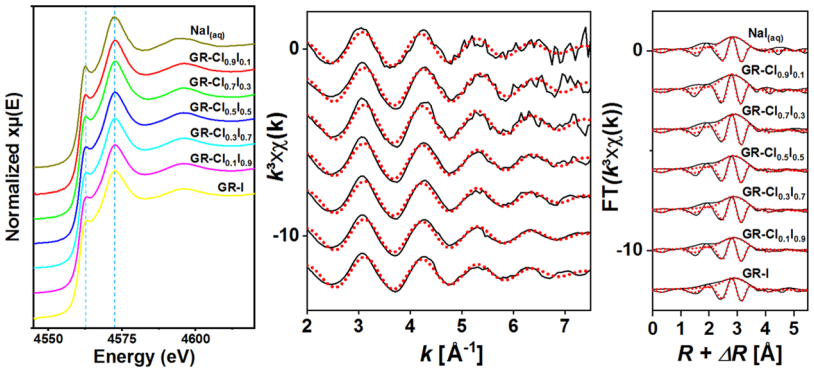

Figure 4. I L_3 edge XANES of the GR samples and the $NaI_{(aq)}$ reference compound (left). Vertical lines in the XANES indicate the position of features discussed in the text. Experimental (solid black line) and modeled (dashed red line) EXAFS spectra (middle) with the corresponding FTs (right) of all samples. Fit results are present in Table 3.

Table 3. Quantitative EXAFS Analysis of GR Samples and the Reference Compound at the I L_3 Edge

sample	FT range[a] [Å^{-1}]	fit range[b] [Å]	shell	N	d [Å]	σ^2 [Å^2]	ΔE_0 [eV]	R_f
GR-$Cl_{0.9}I_{0.1}$	3.3 6.6	2.2 3.7	O_1	6	3.45(18)	0.021(12)	5.8	0.025
GR-$Cl_{0.7}I_{0.3}$	3.3 6.6	2.2 3.7	O_1	6	3.50(18)	0.021(13)	4.1	0.026
GR-$Cl_{0.5}I_{0.5}$	3.3 6.6	2.2 3.7	O_1	6	3.48(19)	0.023(12)	5.0	0.023
GR-$Cl_{0.3}I_{0.7}$	3.3 6.6	2.2 3.7	O_1	6	3.49(18)	0.025(12)	4.5	0.022
GR-$Cl_{0.1}I_{0.9}$	3.3 6.6	2.2 3.7	O_1	6	3.49(15)	0.026(10)	4.6	0.015
GR-I	3.3 6.6	2.2 3.7	O_1	6	3.50(19)	0.027(13)	4.4	0.023
$NaI_{(aq)}$	3.3 6.6	2.2 3.7	O_1	6	3.49(14)	0.025(1)	5.3	0.013

[a]Fourier transformed range. [b]$R + \Delta R$ interval for the fit. N is the coordination number (fixed), d is the interatomic distance, σ^2 is the mean squared displacement (Debye–Waller term), ΔE_0 is the shift in ionization energy with E_0 threshold energy taken as maximum of the first derivative, and R_f is the figure of merit of the fit as reported in ref 56. The number in parentheses indicates the uncertainty.

from octahedral ferric ion slightly increases to ~4.2 Å in GR I (Table 2), but no contribution from iodide located close to only Fe^{3+} could be detected. It is very likely that the loose binding of iodide to the octahedral sheet in GR I results in a distribution of Fe–I interatomic distances around a mean value and thus backscattered EXAFS waves may damp out, precluding the detection of the anionic shell.

The Fe K edge XANES of all GR compounds are comparable (Figure 3) and located between that of $Fe(OH)_2$ and that of magnetite, which indicates the presence of a mixture of ferric and ferrous iron. These findings hint at the absence of the effect of the interlayer composition on the Fe speciation and suggest a rather weak interaction between the interlayer anion and the octahedral sheet, consistent with EXAFS results. The XANES of the magnetite reference compound contains a pre edge feature about ~15 eV before the main absorption edge. This feature is mainly related to 1s → 3d transitions, and the intensity depends on both the site symmetry and electronic properties of Fe.[54] In O_h symmetry, 3d transitions are forbidden, and thus, no pre edge should be observed for octahedrally coordinated Fe, whereas the $1s(a_1) \rightarrow t_2$ transition is allowed in T_d symmetry, implying that a substantial pre edge feature is expected for tetrahedrally coordinated Fe. Accordingly, the XANES of magnetite contains a pre edge feature. The XANES of GR samples hardly contain such pre edge features, which corroborates the presence of Fe in a centrosymmetric environment. In GR, each Fe octahedron shares six edges with neighboring octahedra and OH groups are shifted along the c axis, which decreases the layer thickness and increases the layer lateral dimension. This flattening of FeO_6 octahedra lowers the symmetry from O_h to D_{3d}.[55] Because both point groups are centrosymmetric, no pre edge would be expected in the XANES for Fe in either environment. Yet, fits to the EXAFS data provided a distance separating neighboring octahedral cations of d(Fe–Fe) = 3.20 Å, which is larger than typical values of octahedral sheets, such as in clay minerals ($d \sim 3.05$ Å).[37,38] XAS data thus agree with the flattening of the octahedral sheet in the stacking direction, resulting in a symmetry around Fe of D_{3d}.

3.3.2. I L_3-Edge XAS. The iodine L_3 edge is related to a $2p_{3/2} \rightarrow$ final d state transition. The XANES of the $NaI_{(aq)}$ reference compound displays peaks at ~4562.5 and at ~4572.7 eV (Figure 4). In an earlier study, modeling of experimental XANES recorded for aqueous I^- revealed that the feature at lower energy is very likely related to the presence of H atoms of water binding directly to iodide and almost lying on the iodine–oxygen axis.[57] More recently, Schlegel et al. used an analogy with bromide to attribute both features to the excitation of $2p_{3/2}$ core electrons into the t_{2g} (lower energy) and e_g (higher energy) states of the unoccupied 5d orbitals.[58] The XANES of all GR samples are comparable, suggesting a similar environment in all compounds, irrespective of the interlayer composition (Figure 4). The XANES of these compounds are also comparable to that of the $NaI_{(aq)}$ reference, suggesting that the speciation of iodide in the GR samples is comparable to that of the aqueous ions, thus corroborating a weak interaction with the octahedral sheet. For all compounds, the position and shape of the XANES differ from that reported[58] for I_2, ruling out a change in the iodine oxidation state during $Fe(OH)_2$ conversion into GR. Note that compared to the reported XANES of $NaI_{(cr)}$[59] the presence in significant amounts of that crystalline salt in the GR samples is excluded.

The EXAFS spectra of all investigated GR compounds are likewise very comparable (Figure 4). The amplitude and the position of the oscillation maxima hardly vary with the iodine content, and spectra are also comparable to that of the $NaI_{(aq)}$ reference compound. For the reference and all GR compounds, data could be modeled, considering an O shell containing six atoms at d(I−O) ∼3.50 Å (Table 3). For the aqueous ions, fit results agree with reported data,[43,57,60] including the high structural disorder associated with this shell evidenced by the relatively large Debye−Waller term.[43] These findings are consistent with a high degree of local disorder around iodide located in a water like environment within the GR interlayer, similar to that reported for iodide in (Mg,Zn),Al LDH.[30] The absence of further contribution in the FTs indicates that the coordination between iodide and octahedral cations is not detectable and, therefore, is expected to be weak. These results are consistent with the Fe K edge XAS data hinting at the absence of short range preferential coordination between Fe from the hydroxide sheet and hydrated iodide from the interlayer. These results collectively agree with anionic species very likely electrostatically bound to the octahedral sheet above ferric ions.

3.3.3. Cl K-Edge XAS. The Cl K edge XANES of all reference compounds (Figure 5) are comparable to reported

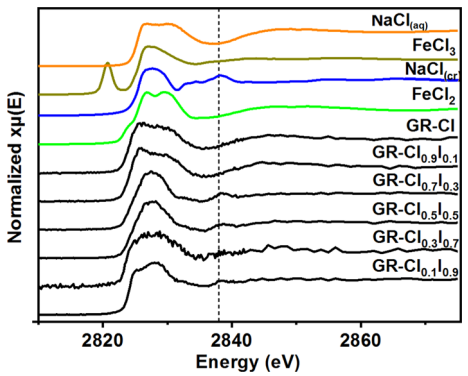

Figure 5. Experimental Cl K edge XANES of the GR samples and four different reference compounds. The dashed line at ∼2838 eV is used to indicate the position of a typical feature present in the XANES of $NaCl_{(cr)}$.

spectra.[43,61,62] The observed differences in XANES of both NaCl compounds are attributed to differences in the short range environment of chloride, being surrounded by six to seven water molecules at d(Cl−O) ∼3.15 Å in $NaCl_{(aq)}$, and by six Na atoms at 2.81 Å in $NaCl_{(cr)}$.[63] The XANES of ferrous and ferric chloride contain either a shoulder or a high intensity pre peak originating from forbidden 1s → 3d transitions, which indicates mixing of metal 3d with Cl 3p orbitals.[64] In addition, the intensity of the pre edge feature gives information on the degree of covalency between the metal and the halide. Its position is affected by the effective charge on Cl and the energy of the metal orbitals involved in bonding. When Cl is not bound to an open shell transition metal, the XANES does not contain any pre edge feature (e.g., NaCl).

The Cl K edge XANES of the GR samples seem to display features depending on the composition of the interlayer (Figure 5). The XANES of GR Cl and GR $Cl_{0.9}I_{0.1}$ have a rather broad edge crest or white line (WL) and are very similar to that of $NaCl_{(aq)}$, suggesting that the Cl speciation in these GR compounds is nearly comparable to those of hydrated chloride ions. The WLs of GR $Cl_{0.7}I_{0.3}$, GR $Cl_{0.5}I_{0.5}$, and GR $Cl_{0.1}I_{0.9}$ are narrower and contain a feature around 2838 eV, which is comparable to that in the XANES of $NaCl_{(cr)}$. Unfortunately, the precipitation of sodium chloride upon sample drying cannot be excluded, implying that the XANES may correspond to a mixture of environments corresponding to Cl associated with GR and to Cl from $NaCl_{(cr)}$. The XANES of GR $Cl_{0.3}I_{0.7}$ is very noisy, hindering a reliable comparison with reference spectra. The presence of $NaCl_{(cr)}$ in some samples hinted from the XANES can be attributed to different efficiencies in the washing procedure during sample prepara tion. Because $NaI_{(cr)}$ and $NaCl_{(cr)}$ are isostructural, non quantitative removal of salt during washing could also have resulted in the formation of $NaCl_{1-x}I_x$.[63,65] Linear combination fitting of experimental XANES using the reference compounds was attempted, but results are not satisfactory (Supporting Information). Specifically, modeled data fail to satisfactorily reproduce the width of the WL and the slope of the rising edge. Dissimilarities in XANES of GR samples with that of the ferric chloride salt in the raising edge region rule out the presence of this compound in GR Cl_xI_{1-x} ($0 \le x \le 1$) samples.

It is very likely that the Cl environment is very similar in all compounds, being hydrated by water molecules and stabilized by weak electrostatic interactions at the center of the interlayer above octahedral trivalent cations.[53] This description is comparable to that observed in this study for I^- within GR compounds and is consistent with Fe K edge XAS data. This weak interaction between hydrated halides and the octahedral sheet is the origin of the high mobility of these anionic species within the interlayer,[53] thereby explaining why Cl^- in GR Cl can be readily exchanged by, for example, SO_4^{2-} present in the contacting water.[35]

4. CONCLUSIONS AND OUTLOOK

GR compounds were prepared by aerial oxidation of $Fe(OH)_2$ in suspension in the presence of chloride and iodide considering various atomic ratios, at constant ionic strength of halogens. All compounds have comparable morphology and exhibit a layered structure. Chemical analyses of the solid phases suggest that the proportions of I or Cl retained by the GR solid phases are correlated to their proportions as dissolved species present during the synthesis; no preferential uptake of I relative to Cl could be observed. Analysis by XRD evidenced a linear increase in basal spacing and an increase in intensity of d_{006} relative to that of d_{003} with increasing iodide content in the starting suspension, which could be attributed to the increasing I^-/Cl^- ratio within the interlayer. Phase segregation and interstratification as well as the compelling presence of pure endmembers in the mixed halide compounds were excluded.

At the short range scale, the GR interlayer composition had no effect on the chemical environment or on the site symmetry of Fe. Furthermore, the short range environment of iodide and chloride associated with GR is comparable to that of the corresponding hydrated ions in aqueous solutions and is not affected by the atomic ratio of anionic species within the interlayer. Consequently, halide anions are present in a water like environment and loosely bound by weak electrostatic interactions to the brucitic sheet. Results collectively point at the formation of a solid solution between the chloride and iodide GR endmembers, which may be facilitated by the crystallization of both compounds in the same space group. These experimental outcomes are currently being comple mented by theoretical calculations at the DFT level.[50,51]

Results of this work show that GR represents a sorbent able to retard the migration of anionic species, such as $^{129}I^-$ and $^{36}Cl^-$ to the far field (see also ref 33). Nevertheless, because the proportions of I^- and Cl^- retained by GR phases depend on their proportion in the contacting aqueous phase, low R_d values can be expected for iodide, which may still result in retention of trace amounts of that species. The retention to pre formed GR via anionic exchange is another relevant iodide uptake mechanism, which needs to be considered for the safety case of a DGR. In this context, the assessment of iodide mobility in the presence of GR in a DGR near field requires a thorough understanding of sorption mechanisms and quanti tative sorption data under relevant geochemical conditions. To this end, the effect on the iodide uptake of various anionic species typically present in the groundwater needs to be scrutinized. Finally, GR may not be thermodynamically stable on the long term and convert to more stable magnetite[7,66] because of, for example, a change in prevailing geochemical conditions. Investigations on the iodide uptake to pre formed GR, including the effect of competing dissolved anionic species, and its fate during the conversion of GR to magnetite are currently ongoing.

Results of this work represent a first step forward in a better understanding of the fate of anionic species present during the formation of LDH compounds at various scales by combining XRD and XAS measurements. Overall findings of this study compare well with that obtained for other LDH compounds [e.g., ZnAl LDH, (Mg/Zn)Al LDH, AFm phases], suggesting that the ability of these compounds to accommodate several anionic species of varying sizes are general properties of LDH and are not specific to any particular chemical composition. It can thus be hypothesized that the substitution of octahedral Fe by other divalent and/or trivalent cations will have no significant impact on the iodine retention by LDH in the presence of other anionic species as long as the endmembers crystallizes in the same space group. This may potentially be of high interest, as such lamellar compounds could also form by corrosion of zero valent iron in remediation technology and because natural ground waters typically contain various cations (e.g., Al^{3+}, Mg^{2+}). In the context of nuclear waste disposal, a variety of other anionic species may be present in a DGR near field during the formation of LDH, such as that typically present in groundwater (e.g., carbonate, sulfate), that introduced during the construction and operation of the repository, and that produced by degradation of cement or the waste matrix itself (e.g., organics and silicates). Further studies would be needed to explore of effect of such competing species on the uptake of anionic fission products by LDH.

■ ASSOCIATED CONTENT

Supporting Information

The Supporting Information is available free of charge at https://pubs.acs.org/doi/10.1021/acs.inorgchem.1c01243.

Full experimental X ray diffractogram of all GR samples, results from alternative fitting strategy of experimental X ray diffractograms, and details on data evaluation of Cl K edge XANES of the GR samples (PDF)

■ AUTHOR INFORMATION

Corresponding Author

Tim Platte − *Institute for Nuclear Waste Disposal (INE), Karlsruhe Institute of Technology (KIT), 76021 Karlsruhe, Germany*; orcid.org/0000 0001 8584 2298; Phone: +49 (0) 721 6082 6048; Email: t.platte@kit.edu

Authors

Nicolas Finck − *Institute for Nuclear Waste Disposal (INE), Karlsruhe Institute of Technology (KIT), 76021 Karlsruhe, Germany*

Stefan Mangold − *Institute for Photon Science and Synchrotron Radiation (IPS), Karlsruhe Institute of Technology (KIT), 76021 Karlsruhe, Germany*

Robert Polly − *Institute for Nuclear Waste Disposal (INE), Karlsruhe Institute of Technology (KIT), 76021 Karlsruhe, Germany*

Horst Geckeis − *Institute for Nuclear Waste Disposal (INE), Karlsruhe Institute of Technology (KIT), 76021 Karlsruhe, Germany*

Author Contributions

The manuscript was written through contributions of all authors.

Notes

The authors declare no competing financial interest.

■ ACKNOWLEDGMENTS

We thank E. Soballa and D. Schild (KIT INE) for SEM analyses. We also thank the Institute for Beam Physics and Technology (IBPT) for the operation of the storage ring, the Karlsruhe Research Accelerator (KARA). This work has received financial support from the German Federal Ministry for Economic Affairs and Energy (BMWi) through the VESPA 2 (Verhalten langlebiger Spalt und Aktivierungsprodukte im Nahfeld von Endlagern unterschiedlicher Wirtsgesteine und Möglichkeiten ihrer Rückhaltung 2) project under contract no. 02 E 11607C.

■ REFERENCES

(1) Guilderson, T. P.; Tumey, S. J.; Brown, T. A.; Buesseler, K. O. The 129 Iodine Content of Subtropical Pacific Waters: Impact of Fukushima and Other Anthropogenic 129 Iodine Sources. *Biogeo sciences* **2014**, *11*, 4839−4852.

(2) Bennett, D. G.; Gens, R. Overview of European Concepts for High Level Waste and Spent Fuel Disposal with Special Reference Waste Container Corrosion. *J. Nucl. Mater.* **2008**, *379*, 1−8.

(3) Hu, Q.; Zhao, P.; Moran, J. E.; Seaman, J. C. Sorption and Transport of Iodine Species in Sediments from the Savannah River and Hanford Sites. *J. Contam. Hydrol.* **2005**, *78*, 185−205.

(4) Bazer Bachi, F.; Tevissen, E.; Descostes, M.; Grenut, B.; Meier, P.; Simonnot, M. O.; Sardin, M. Characterization of Iodide Retention on Callovo Oxfordian Argillites and Its Influence on Iodide Migration. *Phys. Chem. Earth, Parts A/B/C* **2006**, *31*, 517−522.

(5) Tournassat, C.; Gaucher, E. C.; Fattahi, M.; Grambow, B. On the Mobility and Potential Retention of Iodine in the Callovian− Oxfordian Formation. *Phys. Chem. Earth, Parts A/B/C* **2007**, *32*, 539− 551.

(6) Finck, N.; Nedel, S.; Dideriksen, K.; Schlegel, M. L. Trivalent Actinide Uptake by Iron (Hydr)Oxides. *Environ. Sci. Technol.* **2016**, *50*, 10428−10436.

(7) Schlegel, M. L.; Necib, S.; Daumas, S.; Blanc, C.; Foy, E.; Trcera, N.; Romaine, A. Microstructural Characterization of Carbon Steel Corrosion in Clay Borehole Water under Anoxic and Transient Acidic Conditions. *Corros. Sci.* **2016**, *109*, 126−144.

(8) McGill, I. R.; McEnaney, B.; Smith, D. C. Crystal Structure of Green Rust Formed by Corrosion of Cast Iron. *Nature* **1976**, *259*, 200−201.
(9) Stampfl, P. P. Ein Basisches Eisen II III Karbonat in Rost. *Corros. Sci.* **1969**, *9*, 185−187.
(10) Butler, G.; Beynon, J. G. The Corrosion of Mild Steel in Boiling Salt Solutions. *Corros. Sci.* **1967**, *7*, 385.
(11) Abdelmoula, M.; Refait, P.; Drissi, S. H.; Mihe, J. P.; Génin, J. M. R. Conversion Electron Mössbauer Spectroscopy and X Ray Diffraction Studies of the Formation of Carbonate Containing Green Rust One by Corrosion of Metallic Iron in NaHCO3 and (NaHCO3 + NaCl) Solutions. *Corros. Sci.* **1996**, *38*, 623−633.
(12) Feitknecht, W.; Keller, G. Über Die Dunkelgrünen Hydrox yverbindungen Des Eisens. *Z. Anorg. Chem.* **1950**, *262*, 61−68.
(13) Bernal, J. D. The Oxides and Hydroxides of Iron and Their Structural Inter Relationships. *Clay Miner.* **1959**, *4*, 15−30.
(14) Trolard, F.; Génin, J. M. R.; Abdelmoula, M.; Bourrié, G.; Humbert, B.; Herbillon, A. Identification of a Green Rust Mineral in a Reductomorphic Soil by Mössbauer and Raman Spectroscopies. *Geochim. Cosmochim. Acta* **1997**, *61*, 1107−1111.
(15) Taylor, P. A. *Review of Methods for Immobilizing Iodine 129 Arising from a Nuclear Fuel Recycle Plant, with Emphasis on Waste Form Chemistry*; At. Energy Canada Ltd, 1990.
(16) Goldsmith, J. R.; Grossman, C. M.; Morton, W. E.; Nussbaum, R. H.; Kordysh, E. A.; Quastel, M. R.; Sobel, R. B.; Nussbaum, F. D. Juvenile Hypothyroidism among Two Populations Exposed to Radioiodine. *Environ. Health Perspect.* **1999**, *107*, 303−308.
(17) Chong, S.; Peterson, J. A.; Riley, B. J.; Tabada, D.; Wall, D.; Corkhill, C. L.; McCloy, J. S. Glass Bonded Iodosodalite Waste Form for Immobilization of 129I. *J. Nucl. Mater.* **2018**, *504*, 109−121.
(18) Hou, X.; Hansen, V.; Aldahan, A.; Possnert, G.; Lind, O. C.; Lujaniene, G. A Review on Speciation of Iodine 129 in the Environmental and Biological Samples. *Anal. Chim. Acta* **2009**, *632*, 181−196.
(19) Bender Koch, C.; Mørup, S. Identification of Green Rust in an Ochre Sludge. *Clay Miner.* **1991**, *26*, 577−582.
(20) Cui, D.; Spahiu, K. The Reduction of U(VI) on Corroded Iron under Anoxic Conditions. *Radiochim. Acta* **2002**, *90*, 623−628.
(21) Refait, P.; Abdelmoula, M.; GÉnin, J. M. R. Mechanisms of Formation and Structure of Green Rust One in Aqueous Corrosion of Iron in the Presence of Chloride Ions. *Corros. Sci.* **1998**, *40*, 1547−1560.
(22) Finck, N.; Morelová, N.; Cakir Wuttke, P.; Polly, R.; Schild, D. *Korrosions Und Sorptionsprozesse an Stahloberflächen Bei Hohen Temperaturen Und Drücken Im Anaeroben Salinaren Milieu (KORSO)*, 2021.
(23) Boucherit, N.; Hugot Le Goff, A.; Joiret, S. Raman Studies of Corrosion Films Grown on Fe and Fe 6Mo in Pitting Conditions. *Corros. Sci.* **1991**, *32*, 497−507.
(24) Abdelmoula, M.; Trolard, F.; Bourrié, G.; Génin, J. M. R. Evidence for the Fe(II) Fe(III) Green Rust "Fougerite †" Mineral Occurrence in a Hydromorphic Soil and Its Transformation with Depth. *Hyperfine Interact.* **1998**, *112*, 235−238.
(25) Usman, M.; Byrne, J. M.; Chaudhary, A.; Orsetti, S.; Hanna, K.; Ruby, C.; Kappler, A.; Haderlein, S. B. Magnetite and Green Rust: Synthesis, Properties, and Environmental Applications of Mixed Valent Iron Minerals. *Chem. Rev.* **2018**, *118*, 3251−3304.
(26) Jones, A. M.; Murphy, C. A.; Waite, T. D.; Collins, R. N. Fe(II) Interactions with Smectites: Temporal Changes in Redox Reactivity and the Formation of Green Rust. *Environ. Sci. Technol.* **2017**, *51*, 12573−12582.
(27) Van Groeningen, N.; ThomasArrigo, L. K.; Byrne, J. M.; Kappler, A.; Christl, I.; Kretzschmar, R. Interactions of Ferrous Iron with Clay Mineral Surfaces during Sorption and Subsequent Oxidation. *Environ. Sci. Process. Impacts* **2020**, *22*, 1355−1367.
(28) Vinš, J.; Šubrt, J.; Zapletal, V.; Hanousek, F. Preparation and Properties of Green Rust Type Substances. *Collect. Czech. Chem. Commun.* **1987**, *52*, 93−102.
(29) Aimoz, L.; Wieland, E.; Taviot Guého, C.; Dähn, R.; Vespa, M.; Churakov, S. V. Structural Insight into Iodide Uptake by AFm Phases. *Environ. Sci. Technol.* **2012**, *46*, 3874−3881.
(30) Aimoz, L.; Taviot Guého, C.; Churakov, S. V.; Chukalina, M.; Dähn, R.; Curti, E.; Bordet, P.; Vespa, M. Anion and Cation Order in Iodide Bearing Mg/Zn−Al Layered Double Hydroxides. *J. Phys. Chem. C* **2012**, *116*, 5460−5475.
(31) Matschei, T.; Lothenbach, B.; Glasser, F. P. The AFm Phase in Portland Cement. *Cem. Concr. Res.* **2007**, *37*, 118−130.
(32) Nedyalkova, L.; Lothenbach, B.; Geng, G.; Mäder, U.; Tits, J. Uptake of Iodide by Calcium Aluminate Phases (AFm Phases). *Appl. Geochem.* **2020**, *116*, 104559.
(33) Min, J. H.; Baik, M. H.; Lee, J. K.; Jeong, J. T. Sorption of I and Se onto Green Rusts with Different Interlayer Anions, GR(CO 3 2) AND GR(Cl). *J. Nucl. Fuel Cycle Waste Technol.* **2013**, *1*, 57−63.
(34) Bastianini, M.; Costenaro, D.; Bisio, C.; Marchese, L.; Costantino, U.; Vivani, R.; Nocchetti, M. On the Intercalation of the Iodine−Iodide Couple on Layered Double Hydroxides with Different Particle Sizes. *Inorg. Chem.* **2012**, *51*, 2560−2568.
(35) Agnel, M. I.; Grangeon, S.; Fauth, F.; Elkaïm, E.; Claret, F.; Roulet, M.; Warmont, F.; Tournassat, C. Mechanistic and Thermodynamic Insights into Anion Exchange by Green Rust. *Environ. Sci. Technol.* **2020**, *54*, 851−861.
(36) Christiansen, B. C.; Balic Zunic, T.; Petit, P. O.; Frandsen, C.; Mørup, S.; Geckeis, H.; Katerinopoulou, A.; Stipp, S. L. S. Composition and Structure of an Iron Bearing, Layered Double Hydroxide (LDH) − Green Rust Sodium Sulphate. *Geochim. Cosmochim. Acta* **2009**, *73*, 3579−3592.
(37) Manceau, A.; Chateigner, D.; Gates, W. P. Polarized EXAFS, Distance Valence Least Squares Modeling (DVLS), and Quantitative Texture Analysis Approaches to the Structural Refinement of Garfield Nontronite. *Phys. Chem. Miner.* **1998**, *25*, 347−365.
(38) Finck, N.; Schlegel, M. L.; Dardenne, K.; Adam, C.; Kraft, S.; Bauer, A.; Robert, J. L. Structural Iron in Smectites with Different Charge Locations. *Phys. Chem. Miner.* **2019**, *46*, 639−661.
(39) Rothe, J.; Butorin, S.; Dardenne, K.; Denecke, M. A.; Kienzler, B.; Löble, M.; Metz, V.; Seibert, A.; Steppert, M.; Vitova, T.; Walther, C.; Geckeis, H. The INE Beamline for Actinide Science at ANKA. *Rev. Sci. Instrum.* **2012**, *83*, 043105.
(40) Ravel, B.; Newville, M. ATHENA; ARTEMIS, HEPHAESTUS Data Analysis for X Ray Absorption Spectroscopy Using IFEFFIT. *J. Synchrotron Radiat.* **2005**, *12*, 537−541.
(41) Ankudinov, A. L.; Ravel, B.; Rehr, J. J.; Conradson, S. D. Real Space Multiple Scattering Calculation and Interpretation of x Ray Absorption near Edge Structure. *Phys. Rev. B: Condens. Matter Mater. Phys.* **1998**, *58*, 7565−7576.
(42) Aissa, R.; Francois, M.; Ruby, C.; Fauth, F.; Medjahdi, G.; Abdelmoula, M.; Génin, J. M. Formation and Crystallographical Structure of Hydroxysulphate and Hydroxycarbonate Green Rusts Synthetised by Coprecipitation. *J. Phys. Chem. Solids* **2006**, *67*, 1016−1019.
(43) Fulton, J. L.; Schenter, G. K.; Baer, M. D.; Mundy, C. J.; Dang, L. X.; Balasubramanian, M. Probing the Hydration Structure of Polarizable Halides: A Multiedge XAFS and Molecular Dynamics Study of the Iodide Anion. *J. Phys. Chem. B* **2010**, *114*, 12926−12937.
(44) Shannon, R. D. Revised Effective Ionic Radii and Systematic Studies of Interatomic Distances in Halides and Chalcogenides. *Acta Crystallogr., Sect. A: Cryst. Phys., Diffr., Theor. Gen. Crystallogr.* **1976**, *32*, 751−767.
(45) Braithwaite, R. S. W.; Dunn, P. J.; Pritchard, R. G.; Paar, W. H. Iowaite, a Re Investigation. *Mineral. Mag.* **1994**, *58*, 79−85.
(46) Scherrer, P. Bestimmung Der Größe Und Der Inneren Struktur von Kolloidteilchen Mittels Röntgenstrahlen. *Nachrichten von der Gesellschaft der Wissenschaften zu Göttingen*, 1918; pp 98−100.
(47) Holzwarth, U.; Gibson, N. The Scherrer Equation versus the "Debye Scherrer Equation. *Nat. Nanotechnol.* **2011**, *6*, 534.
(48) Kloprogge, J. T.; Frost, R. L. Infrared and Raman Spectroscopic Studies of Layered Double Hydroxides (LDHs). In *Chapter 5 in*

Layered Double Hydroxides: Present and Future; Rives, V., Ed.; Nova Science: New York, 2001.
(49) Zhu, Y.; Elzinga, E. J. Formation of Layered Fe(II) Hydroxides during Fe(II) Sorption onto Clay and Metal Oxide Substrates. *Environ. Sci. Technol.* **2014**, *48*, 4937−4945.
(50) Polly, R.; Finck, N.; Platte, T.; Morelvoa, N.; Heberling, F.; Schimmelpfennig, B.; Geckeis, H. First Principle Investigation of the Incorporation of Trivalent Lanthanides and Actinides in Hydroxycarbonate and Hydroxychloride Green Rust, **2021**. In Preparation.
(51) Polly, R.; Platte, T.; Heberling, F.; Finck, N.; Geckeis, H. Incorporation of Iodide in Hydroxychloride Green Rust. *International Workshop on Theory Frontiers in Actinide Sciences*: Santa Fe, NM, USA, 2020.
(52) Refait, P.; Abdelmoula, M.; Trolard, F.; Génin, J. M. R.; Ehrhardt, J. J.; Bourrié, G. Mössbauer and XAS Study of a Green Rust Mineral; the Partial Substitution of Fe 2+ by Mg 2+. *Am. Mineral.* **2001**, *86*, 731−739.
(53) Sasai, R.; Matsuoka, Y.; Sato, H.; Moriyoshi, C.; Kuroiwa, Y. Abnormally Large Thermal Vibration of Chloride Anions Incorporated in Layered Double Hydroxide Consisting of Mg and Al (Mg/Al = 2). *Chem. Lett.* **2013**, *42*, 1285−1287.
(54) Westre, T. E.; Kennepohl, P.; DeWitt, J. G.; Hedman, B.; Hodgson, K. O.; Solomon, E. I. A Multiplet Analysis of Fe K Edge 1s → 3d Pre Edge Features of Iron Complexes. *J. Am. Chem. Soc.* **1997**, *119*, 6297−6314.
(55) Drits, V. A.; Bookin, A. S.. In *Crystal Structure and X Ray Identification of Layered Double Hydroxides, Layered Do*; Rives, V., Ed.; Nova Science: New York, 2001.
(56) Finck, N.; Dardenne, K.; Geckeis, H. Am(III) Coprecipitation with and Adsorption on the Smectite Hectorite. *Chem. Geol.* **2015**, *409*, 12−19.
(57) Tanida, H.; Kato, K. i.; Watanabe, I. Hydrogen Atom Position in Hydrated Iodide Anion from X Ray Absorption Near Edge Structure. *Bull. Chem. Soc. Jpn.* **2003**, *76*, 1735−1740.
(58) Schlegel, M. L.; Reiller, P.; Mercier Bion, F.; Barré, N.; Moulin, V. Molecular Environment of Iodine in Naturally Iodinated Humic Substances: Insight from X Ray Absorption Spectroscopy. *Geochim. Cosmochim. Acta* **2006**, *70*, 5536−5551.
(59) Cicconi, M. R.; Pili, E.; Grousset, L.; Florian, P.; Bouillard, J. C.; Vantelon, D.; Neuville, D. R. Iodine Solubility and Speciation in Glasses. *Sci. Rep.* **2019**, *9*, 7758.
(60) Maeda, M.; Ohtaki, H. An X Ray Diffraction Study of a Concentrated Aqueous Sodium Iodide Solution. *Bull. Chem. Soc. Jpn.* **1975**, *48*, 3755−3756.
(61) Powell, D. H.; Neilson, G. W.; Enderby, J. E. The Structure of Cl in Aqueous Solution: An Experimental Determination of g ClH (r) and g ClO (R). *J. Phys.: Condens. Matter* **1993**, *5*, 5723−5730.
(62) Konishi, H.; Yamashita, M.; Uchida, H.; Mizuki, J. i. Cl K Edge XANES Spectra of Atmospheric Rust on Fe, Fe Cr and Fe Ni Alloys Exposed to Saline Environment. *Mater. Trans.* **2004**, *45*, 3356−3359.
(63) Abrahams, S. C.; Bernstein, J. L. Accuracy of an Automatic Diffractometer. Measurement of the Sodium Chloride Structure Factors. *Acta Crystallogr.* **1965**, *18*, 926−932.
(64) Rompel, A.; Andrews, J. C.; Cinco, R. M.; Wemple, M. W.; Christou, G.; Law, N. A.; Pecoraro, V. L.; Sauer, K.; Yachandra, V. K.; Klein, M. P. Chlorine K Edge X Ray Absorption Spectroscopy as a Probe of Chlorine−Manganese Bonding: Model Systems with Relevance to the Oxygen Evolving Complex in Photosystem II †. *J. Am. Chem. Soc.* **1997**, *119*, 4465−4470.
(65) Finch, G. I.; Fordham, S. The Effect of Crystal Size on Lattice Dimensions. *Proc. Phys. Soc.* **1936**, *48*, 85−94.
(66) Wang, Z.; Moore, R. C.; Felmy, A. R.; Mason, M. J.; Kukkadapu, R. K. A Study of the Corrosion Products of Mild Steel in High Ionic Strength Brines. *Waste Manag.* **2001**, *21*, 335−341.